Title: A novel ENU-induced ankyrin-1 mutation impairs parasite invasion and increases erythrocyte clearance during malaria infection in mice

Author list and affiliations

Hong Ming Huang[1], Denis C. Bauer[2], Patrick M. Lelliott[3], Andreas Greth[4], Brendan J. McMorran[1], Simon J. Foote[1], Gaetan Burgio[1]*

[1] Department of Immunology and Infectious Disease, John Curtin School of Medical Research, Australian National University, ACT, Australia.

[2] CSIRO, Sydney, NSW, Australia.

[3] IFReC Research Building, Osaka University, 3-1 Yamada-oka, Suita, Osaka 565-0871, Japan.

[4] synaps studios GmbH, Rebmoosweg 73A, CH-5200 Brugg, Switzerland.

Corresponding author*

Dr. Gaetan Burgio

The John Curtin School of Medical Research, Australian National University,

131 Garran Road, ACT 2601, Australia.

Gaetan.burgio@anu.edu.au

+61 2 612 59428

Abstract

Genetic defects in various red blood cell (RBC) cytoskeletal proteins have been long associated with changes in susceptibility towards malaria infection. In particular, while ankyrin (Ank-1) mutations account for approximately 50% of hereditary spherocytosis (HS) cases, an association with malaria is not well-established, and conflicting evidence has been reported. We describe a novel N-ethyl-N-nitrosourea (ENU)-induced ankyrin mutation MRI61689 that gives rise to two different ankyrin transcripts: one with an introduced splice acceptor site resulting a frameshift, the other with a skipped exon. *Ank-1*$^{(MRI61689/+)}$ mice exhibit an HS-like phenotype including reduction in mean corpuscular volume (MCV), increased osmotic fragility and reduced RBC deformability. They were also found to be resistant to rodent malaria *Plasmodium chabaudi* infection. Parasites in *Ank-1*$^{(MRI61689/+)}$ erythrocytes grew normally, but red cells showed resistance to merozoite invasion. Uninfected *Ank-1*$^{(MRI61689/+)}$ erythrocytes were also more likely to be cleared from circulation during infection; the "bystander effect". This increased clearance is a novel resistance mechanism which was not observed in previous ankyrin mouse models. We propose that this bystander effect is due to reduced deformability of *Ank-1*$^{(MRI61689/+)}$ erythrocytes. This paper highlights the complex roles ankyrin plays in mediating malaria resistance.

38 **Introduction**

39 Malaria is a mosquito-borne disease caused by the protozoan *Plasmodium*, responsible for many
40 deaths every year, mostly children [1]. In endemic regions with limited healthcare access, host
41 genetics is one of the major determinants of malaria susceptibility and survival [2-4]. This is evident
42 from the distributions of various genetic polymorphisms in humans, such as Duffy antigen negativity
43 and sickle cell trait, which coincide with malaria distribution [3,5,6]. It is thought that these genetic
44 polymorphisms confer protection against malaria, thus providing a survival advantage in the face of
45 malaria-induced mortality [7,8].

46 In addition, these polymorphisms also provide crucial insights into host-parasite interactions.
47 *Plasmodium* relies on a favourable host environment in order to thrive, many erythrocyte-related
48 polymorphisms have been discovered that interfere with parasite survival thus contributing to
49 malaria resistance. These include polymorphisms that affect the cytoskeleton of erythrocytes, such
50 as Southeast Asian Ovalocytosis (SAO), hereditary elliptocytosis (HE) and spherocytosis (HS) [9-13].
51 Several hypotheses have been proposed for the mechanisms by which they confer malaria
52 protection, including reduced erythrocyte invasion, intra-erythrocytic growth and cytoadherence [8,13-
53 19]. However, due to the heterogeneity of the manifestation of these disorders in the human
54 population, contradicting evidences for resistance mechanisms has often been presented. A study
55 done by Facer [13] showed that only patients carrying certain spectrin mutations have impaired
56 parasite invasion of red blood cells (RBC), but not others that also exhibited HE symptoms. A similar
57 observation was reported by Chishti, et al. [17], where individuals with defective protein 4.1 exhibited
58 intra-erythrocytic growth inhibition, but not those with glycophorin C defects, despite the fact that
59 both defects gave rise to HE. These differences in malaria resistance mechanisms remained largely
60 unexplored, and further studies in this aspect would potentially provide useful insight into host-
61 parasite interactions.

62 The RBC cytoskeletal protein ankyrin-1 (ANK-1), is a 210kDa protein responsible for connecting the
63 spectrin network with the RBC membrane through interactions with Band 3, protein 4.2 and the
64 Rhesus complex [20-22]. Spherocytosis is a genetic disorder where RBCs are abnormally small and are
65 known as spherocytes. ANK-1 mutations account for more than 50% of human HS cases [23]. However,
66 similar to SAO and HE, HS is a heterogeneous disorder where the symptoms vary greatly depending
67 on the mutations. The disorder can range from asymptomatic through to severe anaemia requiring
68 splenectomy [24]. Despite a possible association with malaria, HS is actually common in Northern
69 European and Japanese populations with frequency of about 1 in 2000 individuals [25-28], but much
70 rarer in other populations [29]. Nevertheless, several *in vitro* and *in vivo* studies have repeatedly
71 reported association between HS and malaria resistance, and several mechanisms have been
72 suggested. An *in vitro* study done by Schulman, et al. [16] using RBCs from HS patients suggested that
73 parasite invasion and growth in these erythrocytes was impaired. This is further supported by
74 studies done in mice with ankyrin mutations. Both *Ank-1*$^{(nb/nb)}$ and *Ank-1* $^{(MRI23420/+)}$ have shown
75 inhibited intra-erythrocytic growth and erythrocyte invasion possibly due to spectrin and ankyrin
76 deficiency, respectively [30,31]. On the other hand, another mutation described by Rank, et al. [32], *Ank-*
77 *1*$^{1674/+}$, parasite invasion appeared to be normal in these erythrocytes. Instead, increased erythrocyte
78 fragility was proposed as a contributing factor for increased malaria resistance [32]. Taking these
79 observations together, it is possible that disruption to erythrocyte cytoskeletons can mediate
80 multiple mechanisms of resistance.

81 In a large phenotypic N-ethyl-N-nitrosourea (ENU) mutagenesis screen, using either abnormal red
82 cells or resistance to malaria as to the screened phenotypes, we identified many novel mutations
83 that give rise to RBC abnormalities and consequently malaria resistance in mice. We report here an
84 ENU-induced mutation in the ankyrin-1 gene (*Ank-1*$^{(MRI61689)}$) which was found to exhibit a HS-like
85 phenotype, with significantly lower RBC volumes, increased osmotic fragility and decreased
86 deformability. *Ank-1*$^{(MRI61689)}$ also confers resistance towards *Plasmodium chabaudi adami* infection

87 in mice, and *Ank-1*$^{(MRI61689/+)}$ mice were shown to show both reduced merozoite invasion and
88 increased RBC clearance, possibly as a consequence of reduced red blood cell deformability.

89

90 **Results**

91 The MRI61689 mutation gives rise to an hereditary spherocytosis-like phenotype

92 The G1 mouse carrying the MRI61689 mutation was initially identified from an ENU suppressor
93 screen for the recessive mutation db/db. The G1 MRI61689 exhibited abnormal blood parameters on
94 an ADVIA haematological analyser, with reduced MCV of 48.6fL compared to the background of
95 53.3±0.5fL. This MCV values from the B6.BKS(D)-Lepr^{db}/J background is comparable to C57BL/6 mice.
96 We crossed the G1 founder mouse with B6.BKS(D)-Lepr^{db}/J to produce G2 mice where approximately
97 half of the animals exhibited an abnormal phenotype (Table 1). The affected G2 progeny, which
98 were obligate heterozygotes for the ENU-induced mutation, showed reduction in MCV (46.1±0.2fL)
99 compared to unaffected progeny (51.4±0.4fL), lower mean corpuscular haemoglobin (MCH)
100 (13.5±0.1pg compared to 14.6±0.1pg of wild-type), elevated RBC count (11.1±0.1x10^{9} cells/ml
101 compared to 10.5±0.1x10^{9} cells/ml of wild-type) (Table 1). No differences were observed for total
102 haemoglobin (HB), mean corpuscular haemoglobin concentration (MCHC), white blood cell (WBC)
103 count, platelets count (PLT) or reticulocyte percentage (Table 1).

104 However, when two affected mice were intercrossed, a quarter of the pups were found to die within
105 1 week postnatally, suggesting homozygosity for MRI61689 might be incompatible with life. Blood
106 smears were taken from these pups and compared with the other affected and unaffected mice. The
107 heterozygotes have slightly smaller RBCs but no target cells or spherocytes were observed (Figure
108 1a). Conversely, homozygous mice had significantly smaller RBCs with anisocytosis, fragmented RBCs,
109 acanthocytes and reticulocytosis (Figure 1a). Under SEM, RBCs of heterozygous mice seemed to have
110 less distinct discoid shape, but otherwise no distinguishing features were observed. (Figure 1b). On

111 the other hand, the RBCs of homozygous mice appeared very deformed, acanthocytic and appeared
112 to lack the discoid shape (Figure 1b).

113 When subjected to osmotic stress, RBCs of heterozygous mice showed significantly increased
114 fragility compared to wild-type erythrocytes (with 50% haemolysis at approximately 5.6 g/L
115 compared to 4.5 g/L of wild-type) (Figure 1c). The RBC deformability was assessed using an *in vitro*
116 spleen retention assay by filtering RBCs through a layer of beads with varying sizes. This is thought to
117 model splenic filtration *in vivo*, with retention thought to indicate reduced deformability. As shown
118 in Figure 1d, up to 70% of the RBCs from heterozygous MRI61689 mice were retained within the
119 bead layer compared to 3.5% of wild-type RBCs, suggesting a significantly reduced RBC deformability
120 in the presence of this ankyrin mutation.

121

122 MRI61689 carries a splice site mutation in *Ank-1* gene resulting in an alternative transcript and exon
123 skipping

124 To identify the causative mutation responsible for this abnormal RBC count, we sequenced the
125 exomes of 2 heterozygous mice. Exome sequencing revealed a number of variants. These were
126 prioritised based on filters as shown in Table 2. Through further genotyping using Sanger sequencing,
127 a mutation in *Ank-1* gene was found to correlate with all the affected mice and was proven to
128 segregate perfectly with the reduced MCV for over 3 generations of mouse crosses. The mutation
129 was found in the 17-18 intron of *Ank-1* gene, with T to A transversion 11 base pair upstream of exon
130 18 (IVS17-11T>A) (Figure 2a). This is situated in the ankyrin-repeats domain involved in band 3
131 binding. We proposed that the mutation introduced a new acceptor splice site for exon 18,
132 potentially leading to a frameshift mutation.

133 To assess this hypothesis, transcript analysis was performed. Embryonic liver RNA was extracted,
134 cDNA was synthesized and PCR-amplified using primers listed in the experimental procedures. Figure

135 2b shows the PCR products of embryonic liver cDNA from non-mutant, *Ank-1*$^{(MRI61689/+)}$ and *Ank-*
136 *1*$^{(MRI61689/MRI61689)}$ when amplified using primer set 1, which covers exon 17 to 21. Bands of
137 approximately 400bp can be observed in all the genotypes, but *Ank-1*$^{(MRI61689/MRI61689)}$ also exhibited a
138 second smaller product of approximately 300bp length. We proposed that this second band resulted
139 from exon skipping. Sanger sequencing of these PCR products revealed that the 300bp product
140 lacked exon 18, confirming that the exon 18 was skipped, and exon 19 was directly connected to
141 exon 17 during transcription (Figure 2c). This transcript is predicted to produce a shortened, in-
142 frame 207kDa ANK-1 protein.

143 To examine the effect of MRI61689 mutation in heterozygous mice, we further designed a primer set
144 containing the predicted acceptor splice site (primer set 2). Figure 2d shows that the mutant
145 transcript is only present in *Ank-1*$^{(MRI61689/+)}$ and *Ank-1*$^{(MRI61689/MRI61689)}$ mice, as predicted. Further
146 Sanger sequencing revealed an insertion of 11bp into the transcript adding an additional donor
147 splicing site and causing a frameshift mutation in the exon that would result in a premature stop
148 codon at amino acid position 724, as illustrated in Figure 2e, thus giving rise to a truncated protein of
149 78.5kDa. Therefore the homozygous mice exhibit a mutation at 11 bp upstream of the exon 18
150 donor splicing site resulting in two alternative transcripts: the skipping of exon 18 and an 11bp
151 insertion and creation of an additional donor splicing site leading to frameshift mutation that would
152 result in a premature stop codon and a truncated protein.

153 We hypothesize that this mutation would reduce the *Ank*-1 expression levels. We assessed this
154 hypothesis by examining the gene expression levels of *Ank-1* in embryonic liver using qPCR at mRNA
155 level and Western blotting at protein level in mature RBCs. As shown in Figure 3a, *Ank-1* mRNA
156 levels in both *Ank-1*$^{(MRI61689/+)}$ and *Ank-1*$^{(MRI61689/MRI61689)}$ E14 embryonic livers were significantly
157 reduced, up to 60% and 80% reduction compared to the wild-type, respectively. However, no
158 significant reduction in the full length ANK-1 (210kDa) protein levels was observed in both
159 Coomassie and Western blotting (Figure 3b-d). No truncated form of ANK-1 (78.5kDa) was observed

160 in *Ank-1*$^{(MRI61689/+)}$ erythrocytes. Furthermore, no reduction was observed for the protein levels of
161 other cytoskeletal proteins, including Band 3, protein 4.2, alpha- and beta-spectrin (Figure 3b and 3c,
162 Supp. Figure 1). This suggested that erythrocyte protein levels might be compensated by the WT
163 allele in *Ank-1*$^{(MRI61689/+)}$ mice, and the reduction in *Ank-1* mRNA levels did not seem to affect the
164 protein levels.

165

166 *Ank-1*$^{(MRI61689/+)}$ mice are resistant to *Plasmodium chabaudi* infection

167 We hypothesized that the *Ank-1*$^{(MRI61689)}$ mutation confers malaria resistance. The malaria
168 susceptibility of *Ank-1*$^{(MRI61689/+)}$ mice was examined by injecting a lethal dose of *Plasmodium*
169 *chabaudi adami DS*, a murine strain of malaria that models the *Plasmodium falciparum* erythrocytic
170 stage [33]. The *Ank-1*$^{(MRI61689/+)}$ mice exhibited significantly lower peak parasitemia, with only
171 approximately 13% parasitemia compared to 52% parasitemia of wild-type (Figure 4a) but no delay
172 in the appearance of parasites was observed. In addition, *Ank-1*$^{(MRI61689/+)}$ have a significantly
173 increased survival rate, where all the *Ank-1*$^{(MRI61689/+)}$ mice survived the infection (Figure 4b)
174 compared to the 16% survival of wild-type mice. Since *Ank-1*$^{(MRI61689)}$ directly affects the red cell
175 (cytoskeletal protein), we hypothesized that the resistance was likely due to a RBC-autonomous
176 effect. Therefore, we postulated three mechanisms of *P. chabaudi* resistance in *Ank-1*$^{(MRI61689/+)}$ mice.
177 Firstly, the maturation of parasite inside the *Ank-1*$^{(MRI61689/+)}$ erythrocytes could be impaired leading
178 to reduced growth and death of parasites [31]. Secondly, the *Ank-1*$^{(MRI61689/+)}$ erythrocytes might be
179 resistant to merozoite invasion, which resulted in reduced parasitemia and delayed course of
180 infection [15]. Finally, the infected *Ank-1*$^{(MRI61689/+)}$ erythrocytes might more prone to destruction during
181 the course of infection (increased clearance), thus posing a challenge for the parasite to establish a
182 successful infection [34].

183

184 *Ank-1*$^{(MRI61689)}$ does not impair the intra-erythrocytic growth of *P. chabaudi*.

185 To elucidate the possible mechanisms of resistance, the effect of the *Ank-1*$^{(MRI61689/+)}$ mutation on
186 parasite intra-erythrocytic growth was investigated using the TUNEL assay at 1-10% parasitemia.
187 TUNEL detects DNA fragmentation, a marker for apoptosis or necrosis. In conjunction with a DNA
188 fluorescent dye, DAPI, it is possible to detect dying parasites in the erythrocytes (Figure 4c) [31,35]. We
189 measured the TUNEL-positivity of *P. chabaudi* in *Ank-1*$^{(MRI61689/+)}$ erythrocytes during the late
190 trophozoite stage of the infections, which was the portion of the parasite lifecycle affected by the
191 *Ank1* mutation in the *Ank-1*$^{(MRI23420/+)}$ line. As shown in Figure 4d, no differences was observed in the
192 percentage of TUNEL-positive parasites in both wild-type and *Ank-1*$^{(MRI61689/+)}$ erythrocytes (24.7 ± 2.3%
193 in *Ank-1*$^{(MRI61689/+)}$ mice compared to 29.5 ± 2.9% in wild-type). This indicated that *Ank-1*$^{(MRI61689)}$ did
194 not impair parasite intra-erythrocytic growth.

195

196 *Ank-1*$^{(MRI61689/+)}$ erythrocyte is resistant to *P. chabaudi* invasion, and have increased clearance from
197 circulation

198 Erythrocyte invasion and clearance were assessed via an *in vivo* erythrocyte tracking (IVET) assay.
199 Labelled blood of wild-type and *Ank-1*$^{(MRI61689/+)}$ mice were injected into infected wild-type mice
200 during merozoite invasion to examine the ability of *Plasmodium chabaudi* to invade and grow within
201 erythrocytes of both genotypes. The result compared the percentage of parasitized cells of both
202 genotypes and expressed as a ratio of parasitemia in *Ank-1*$^{(MRI61689/+)}$ RBC to wild-type RBC
203 populations. As shown in Figure 4e, lower parasitemia ratio (approximately 0.55) was observed from
204 30 minutes after injection with labelled blood, and was consistently lower in *Ank-1*$^{(MRI61689/+)}$ blood
205 over 36 hours post injection, which indicates a lower invasion rate into the *Ank-1*$^{(MRI61689/+)}$ RBCs.
206 Additionally, the remaining proportion of labelled RBCs was also monitored over the course of the
207 assay. A significant reduction of *Ank-1*$^{(MRI61689/+)}$ erythrocytes in infected mice compared to wild-type
208 erythrocytes was observed, with up to a 45% reduction in *Ank-1*$^{(MRI61689/+)}$ RBC number compared

209 with wild-type (Figure 4f). On the other hand, a smaller reduction was observed for *Ank-1*$^{(MRI61689/+)}$
210 erythrocytes compared to wild-type in uninfected mice, suggesting *Ank-1*$^{(MRI61689/+)}$ RBCs are more
211 likely to get cleared from circulation during malaria infection. As the percentage of infected
212 erythrocytes was low (5-20%) (Supp. figure 1), this indicates that the majority of the RBCs getting
213 cleared were uninfected RBCs, possibly as a result of bystander effect. This experiment suggested
214 that two possible mechanisms of resistance are both operating to produce the lower parasitemia
215 and increased survival in *Ank-1*$^{(MRI61689/+)}$ mice, the reduction of parasite invasion and increased
216 clearance of *Ank-1*$^{(MRI61689/+)}$ RBCs.

217

218 **Discussion**

219 We report a novel mutation in *Ank-1* gene, MRI61689, causing a hereditary spherocytosis-like
220 phenotype, with reduced MCV, increased osmotic fragility and reduced deformability. MRI61689 is
221 an intronic mutation between exon 17 and 18 where two possible splice variants could arise, one
222 has an introduced acceptor site resulting a frameshift, whereas the other consists of a skipped exon
223 18. The *Ank-1* mRNA levels were reduced, but no reduction in protein levels were observed. The
224 predicted truncated form (78.5kDa) was also not observed. *Ank-1*$^{(MRI61689/+)}$ mice also have increased
225 resistance to *Plasmodium chabaudi* infections, and the erythrocyte invasion was impaired but the
226 intra-erythrocytic growth appeared normal. The *Ank-1*$^{(MRI61689/+)}$ RBCs were also more likely to be
227 cleared from circulation during infection, an observation independent of number of parasitized
228 erythrocytes.

229 In comparison of *Ank-1*^{MRI61689} mice to other previously described *Ank-1* mouse models, they
230 appeared comparable to *Ank-1*^{MRI23420} mice, but more severe than *Ank-1*^{1674} and *Ank-1*^{nb} mice. More
231 specifically, most homozygous *Ank-1*$^{(MRI61689)}$ mice died within a week after birth, similar to
232 homozygous *Ank-1*^{MRI23420} mice, while homozygous *Ank-1*^{1674} and *Ank-1*^{nb} mice were viable [30,32].
233 However, no notable differences were observed in heterozygous *Ank-1*^{MRI61689} mice in terms of their

234 RBC microcytosis, morphology and susceptibility to osmotic stress compared to heterozygous *Ank-*
235 *1*^{1674} and *Ank-1*^{MRI23420} mice [31,32]. However, similar to *Ank-1*$^{1674/+}$ mice and unlike *Ank-1*$^{(MRI23420/+)}$ mice,
236 *Ank-1*$^{(MRI61689/+)}$ mice exhibited similar levels of ankyrin and other RBC cytoskeletal protein to wild-
237 type, which might suggest compensation by the wild-type allele, and thus warrants further studies.

238 In humans, many *ANK-1* mutations that result in frameshift have been described, most of which
239 situated in the band 3 binding domain towards the N terminus [36,37]. While no *Ank-1*$^{(MRI61689)}$
240 homologous mutation has been described in humans, a frameshift mutation has been reported to be
241 in the exon 17, called Ankyrin Osaka I, which gave rise to symptomatic HS [37]. Furthermore, exon
242 skipping in human *ANK-1* gene has also been documented. Edelman, et al. [38] reported a HS patient
243 exhibiting a severe ankyrin-deficient HS due to an introduction of a new splice acceptor site for exon
244 17, known as ankyrin^{Ankara}. Under further examination, this mutation was found to give rise to
245 multiple splice forms, including insertions and skipped exons. Most splice forms with insertion were
246 expected to cause frameshift, potentially leading to premature termination of ankyrin [38]. This finding
247 is in agreement with what we observed for *Ank-1*$^{(MRI61689/MRI61689)}$ mice, where frameshift caused by
248 new splice acceptor site, leading to high mortality rate with severe HS-like phenotype in *Ank-*
249 *1*$^{(MRI61689/MRI61689)}$ mice. It is likely that the surviving *Ank-1*$^{(MRI61689/MRI61689)}$ mice relied on the exon-
250 skipping splice form to produce in-frame functional *Ank-1* proteins. However, further studies are
251 required for support this hypothesis.

252 In terms of the response to malaria infection, *Ank-1*$^{(MRI61689/+)}$ mice exhibited similar degree of
253 malaria resistance as *Ank-1*$^{(MRI23420/+)}$ and *Ank-1*$^{1674/+}$ mice, with at least 30-40% reduction in
254 parasitemia and increased survival [31,32], and unlike *Ank-1*$^{nb/+}$ mice with only 10% reduction [30].
255 Previous studies suggested the reduction in erythrocyte invasion and intra-erythrocytic growth to be
256 the major resistance mechanisms [30,31]. However, normal parasite invasion was reported in *Ank-1*$^{1674/+}$
257 mice [32]. As a result, we have explored the potential mechanisms of *Ank-1*$^{MRI61689/+}$ mice in this study
258 in attempt to elucidate the complex roles ankyrin plays during malaria infections.

259 First, we report that *Ank-1*$^{(MRI61689/+)}$ mice exhibit normal parasite intra-erythrocytic growth (Figure
260 4d), in contrast to *Ank-1*$^{(MRI23420/+)}$ mice. TUNEL assay detects the presence of DNA fragmentation
261 which occurs during apoptosis and necrosis [39], which indicates dying parasites in RBCs [35]. McMorran,
262 et al. [35] reported TUNEL-positive parasites in C57BL/6 wild-type mice at a level consistent with the
263 observations in this study. On the other hand, Greth, et al. [31] reported a lower TUNEL-positive in
264 their SJL/J wild-type mice, which most likely due to differences in the genetic background of
265 experimental mice. Nevertheless, we did not observe abnormal parasite morphology under light
266 microscopy unlike *Ank-1*$^{(MRI23420/+)}$ mice, which support the deductions of parasite death from the
267 TUNEL assays. We also did not observe a difference in gametocyte numbers (Supp. Figure 2),
268 indicating gametocytogenesis was not affected. However, we cannot exclude the possible growth
269 retardation that might occur in other parasite stages, which were not tested in this study.

270 In terms of parasite invasion, *Ank-1*$^{(MRI61689/+)}$ RBCs were found to be more resistant to merozoite
271 invasion as shown in the IVET assay (Figure 4e). The *Ank-1*$^{(MRI61689/+)}$ erythrocytes were less infected
272 compared to the wild-type 30 minutes after injection during merozoite invasion, and stayed
273 consistently lower compared to wild-type throughout the erythrocytic cycle. This reduction in
274 invasion has also been observed in *Ank-1*$^{(MRI23420/+)}$ mice [31]. In contrast, Rank, et al. [32] reported no
275 difference in parasite invasion for *Ank-1*$^{1674/+}$ mice, indicating a different effect mediated by *Ank-1*^{1674}
276 mutation compared to *Ank-1*$^{(MRI23420)}$ and *Ank-1*$^{(MRI61689)}$ mutations.

277 From these comparisons with other ankyrin mouse models, it is evident that RBC cytoskeleton plays
278 an important yet complex role during malaria infections. However, the exact mechanism for each of
279 these different phenotypes for each ankyrin haplotype remains elusive, different ankyrin mutations
280 can exert different effects on the parasites depending on the location of the mutations, giving rise to
281 multiple resistance mechanisms. This hypothesis is also consistent with the heterogeneous HS
282 symptoms associated with ankyrin mutations, which highlights the complicated interactions
283 between RBC cytoskeletons and malaria parasites.

284 On the other hand, one important observation from the IVET assay is the rapid clearance of *Ank-*
285 *1*$^{(MRI61689/+)}$ erythrocytes from the circulation within 36 hours post-injection, up to 40% of the initial
286 RBC number (Figure 4f). However, at this timepoint the parasitemia of the host mice was only 5-20%
287 (Supp. Figure 3), therefore the rate of RBC clearance cannot be explained by the clearance of
288 parasitized RBCs, instead, it is likely that the majority of the RBCs being cleared were uninfected. In
289 comparison, no loss was observed for wild-type erythrocytes in both infected and uninfected mice.
290 Since, in these experiments both wild-type and *Ank-1*$^{(MRI61689/+)}$ blood were subjected to the same
291 host environment simultaneously, it implies that the clearance of *Ank-1*$^{(MRI61689/+)}$ erythrocytes is cell
292 autonomous, rather than due to other effects of the host animal during infectiom. This is further
293 supported by the observation that increased *Ank-1*$^{(MRI61689/+)}$ erythrocyte clearance in uninfected
294 mice, indicating that *Ank-1*$^{(MRI61689/+)}$ erythrocytes were predisposed for clearance. This is the first
295 observation of increased, uninfected RBC clearance associated with an ankyrin mutation. Bystander
296 clearance is typically observed in inflammation, such as during sepsis [40], and is thought to cause
297 severe malaria anaemia during malaria infection in humans through the destruction of normal
298 uninfected RBCs [41,42]. It is possible that *Ank-1*$^{(MRI61689)}$ causes a more exaggerated bystander effect
299 during malaria infection, leading to a further reduction of *Ank-1*$^{(MRI61689/+)}$ erythrocyte numbers.

300 Reduced RBC deformability was proposed to be one of the mechanisms of bystander clearance
301 during malaria anaemia through phagocytosis and splenic filtration [43,44]. From the *in vitro* spleen
302 retention assay (Figure 1d), *Ank-1*$^{(MRI61689/+)}$ erythrocytes exhibited reduced deformability, making
303 them more likely to be retained in the filter layer, which is likely to promote their destruction in *in*
304 *vivo* settings. Therefore, we proposed that *Ank-1*^{MRI61689} mutation causes alteration to the
305 erythrocyte, which renders them more likely to be cleared from the circulation.

306 In summary, we report that ENU-induced *Ank-1*^{MRI61689} mutation causes an HS-like phenotype in mice,
307 and confers significant resistance to *P. chabaudi* infection. We propose that *Ank-1*$^{(MRI61689/+)}$
308 erythrocytes are significantly resistant to parasite invasion but appeared to support normal

309 trophozoite development, although it is possible that this mutation might affect growth of other
310 parasite stages. We also described a novel observation of increased RBC clearance associated with
311 this ankyrin mutation. This study emphasizes the importance of RBC cytoskeletal proteins in
312 mediating multiple complex mechanisms of resistance towards malaria, which provide further
313 insights to the complex interaction between the host and parasites.

314

315 **Methods and Materials**

316 Mice and Ethics Statement

317 All mice used in this study were housed with 12 hour light-dark cycle under constant temperature at
318 21 °C. All procedures were conformed to the National Health and Medical Research Council (NHMRC)
319 Australian code of practice. Experiments were performed under ethics agreement AEEC A2014/54,
320 which were approved by the Australian National University animal ethics committees.

321

322 ENU Mutagenesis and Dominant Phenotype Screening

323 B6.BKS(D)-Lepr^{db}/J male mice were injected intraperitoneally with two dose of 100 mg/kg ENU
324 (Sigma-Aldrich, St Louis, MO) at one week interval for a recessive suppressor screen of db/db
325 mutation. The treated males (G0) were crossed to females from the isogenic background to produce
326 the first generation progeny (G1). The seven-week-old G1 progeny were bled and analysed on an
327 Advia 120 Automated Haematology Analyser (Siemens, Berlin, Germany) to identify abnormal red
328 blood cell count. Mouse carrying MRI61689 mutation was identified with a "mean corpuscular
329 volume" (MCV) value three standard deviations lower from other G1 progeny. It was crossed with
330 B6.BKS(D)-Lepr^{db}/J mice to produce G2 progeny to test the heritability of the mutations and the
331 dominance mode of inheritance. Mice that exhibited low MCV (<48fL) were selected for whole

332 exome sequencing and genotyping. This abnormal red blood cell count was unrelated to the obesity
333 phenotype.

334

335 Microscopy

336 For light microscopy, cells were briefly fixed in methanol for one minute and air-dried before being
337 stained in a 10% Giemsa solution (Sigma-Aldrich, St Louis, MO) at pH 7.4 for 10 minutes. For
338 scanning electron microscopy (SEM), fresh blood was first fixed immediately upon drawing in 3%
339 EM-grade glutaraldehyde (Sigma-Aldrich, St Louis, MO) overnight at 4°C. The samples were washed
340 with mouse tonicity phosphate buffered saline (MT-PBS) (150mM NaCl, 16mM Na_2HPO_4, 4mM
341 NaH_2PO_4, pH 7.4) 3 times, 10 minutes soak each. The cells were then adhered to the cover slips with
342 0.1% polyethyleneimine (PEI) for 10 minutes, before washing off with MT-PBS. The cells were then
343 dried serially using 30%, 50%, 70%, 80%, 90%, 100%, 100% ethanol, each with 10 minutes soak. The
344 cells were then soaked in 1:1 ethanol: hexamethyldisilazane solution for 10 minutes, followed by 2
345 washes with 100% hexamethyldisilazane, each 10 minutes. The coverslips were then air-dried
346 overnight and coated with gold and examined under JEOL JSM-6480LV scanning electron microscope.

347

348 Osmotic Fragility Measurement

349 To assess the susceptibility of RBC membrane to osmotic stress, 5µl of mouse whole blood was
350 diluted 100-fold with phosphate buffer (pH 7.4) containing 0 to 10g/L of sodium, and incubated for
351 at least 10 minutes at room temperature. The cells were centrifuged at 800g for 3 minutes, and the
352 supernatant, which contains free haemoglobin, was measured at 540nm to assess the degree of
353 haemolysis. The absorbance values were expressed as percentage of haemolysis, with haemolysis at
354 0g/L sodium considered as 100% lysis.

355

356 *In vitro* spleen retention assay

357 The RBC deformability of both wild-type and *Ank-1*$^{(MRI61689/+)}$ were assessed according to the protocol
358 described previous by Deplaine, et al. [45] with modifications. Briefly, RBCs from wild-type and *Ank-*
359 *1*$^{(MRI61689/+)}$ mice were stained with 10µg/ml of either hydroxysulfosuccinimide Atto 633 (Atto 633) or
360 hydroxysulfosuccinimide Atto 565 (Atto 565) (Sigma-Aldrich, St Louis, MO), followed by three
361 washes with in MTRC (154mM NaCl, 5.6mM KCl, 1mM $MgCl_2$, 2.2mM $CaCl_2$, 20mM HEPES, 10mM
362 glucose, 4mM EDTA, 0.5% BSA, pH 7.4, filter sterilized). The stained RBCs were mixed in equal
363 proportion and diluted with unstained wild-type RBCs to give approximately 10-20% of the sample
364 being labelled RBCs. The samples were further diluted to 1-2% haematocrit with MTRC, before
365 passing through spleen retention filter bed. The pre-filtered and post-filtered samples were analysed
366 on BD LSRFortessa (BD Biosciences, Franklin Lakes, NJ) flow cytometer to determine the proportion
367 being retained in the filter bed.

368

369 Whole exome sequencing

370 DNA from two G2 mice carrying the abnormal red blood cell parameters (MCV <48fL) were extracted
371 with Qiagen DNeasy blood and tissue kit (Qiagen, Venlo, Netherlands) for exome sequencing as
372 previous described [46]. Briefly, at least 10µg of DNA was prepared for exome enrichment with Agilent
373 Sure select kit paired-end genomic library from Illumina (San Diego, CA), followed by high
374 throughput sequencing using a HiSeq 2000 platform. The bioinformatics analysis was conducted
375 according to the variant filtering method previously described by Bauer, et al. [47]. Private variants
376 that were shared between the two mutants but not with other B6.BKS(D)-Lepr^{db}/J, C57BL/6 mice or
377 previously described ENU mutants were annotated using ANNOVAR [48]. Private non-synonymous
378 exonic and intronic variants within 20 bp from the exon spicing sites were retained as potential
379 candidate ENU mutations.

380

381 PCR and Sanger sequencing

382 DNA from mutant mice were amplified through PCR with 35 cycles of 30 seconds of 95^0C
383 denaturation, 30 seconds of 56-58^0C annealing and 72^0C elongation for 40 seconds. The primers
384 used in the PCR are described as below. The PCR products were examined with agarose gel
385 electrophoresis before being sent to the Australian Genome Research Facility (AGRF) in Melbourne,
386 Australia, for Sanger sequencing. Logarithm of odds (LOD) score was calculated based on the
387 number of mice that segregated with the candidate mutations.

388 Primers:

389 *Acp5*-F: 5'-CAGAAGGATGCCTTTGGGTA-3'; *Acp5*-R: 5'-ACCAGCGCTTGGAGATCTTA-3'

390 *Kcnk1*-F: 5'-GGGCCTTTTCCTCCTTACAGA-3'; *Kcnk1*-R: 5'-CAGGAAACGGTGACAAATCC-3'

391 *Epas1*-F: 5'-GGAAGCCAGAACTTCGATGA-3'; *Epas1*-R: 5'-GTAGTGTTCCCTGGGGTGT-3'

392 *Picalm*-F: 5'-TCACTGAATGTAATTGGGATATCAT-3'; *Picalm*-R: 5'-CACCCTCTCTTCACTTTTGTG-3'

393 *Socs6*-F: 5'-CCGCTTTGTTATCCGTCAGT-3'; *Socs6*-R: 5'-TGGCAGCAAAGACTTCAATG-3'

394 *Ank1*-F: 5'-TCCCTGGCTTAAAGTTGGTG-3'; *Ank1*-R: 5'-CTCTCCCTTAGCTGCATTCC-3'

395

396 Quantitative PCR and cDNA sequencing

397 RNA was isolated from embryonic livers of E14 embryos using Qiagen RNeasy kit (Qiagen, Venlo,
398 Netherlands), followed by cDNA synthesis using Transcriptor High Fidelity cDNA Synthesis Kit (Roche,
399 Basel, Switzerland). Quantitative PCR was carried out on ViiA™ 7 Real-Time PCR System (Thermo
400 Scientific, Waltham, MA). The $\Delta\Delta C_T$ method [49] was used to determine the cDNA levels of *Ank-1* and
401 the housekeeping gene β-actin and expressed as a fold-change of the mutants to the wild-type. The

402 primers used for *Ank-1* gene spanned exon 2 to 4: *Ank-1*-F: 5'-TAACCAGAACGGGTTGAACG-3'; *Ank-1*-
403 R: 5'-TGTTCCCCTTCTTGGTTGTC-3'; β-Actin-F: 5'- TTCTTTGCAGCTCCTTCGTTGCCG-3'; β-Actin-R: 5'-
404 TGGATGCGTACGTACATGGCTGGG-3'.

405 To characterize the effect of MRI61689 mutation, cDNA were amplified through PCR using two
406 primers set were design as shown below: Primer set 1 was designed to amplify wild-type *Ank-1*
407 transcript, whereas primer set 2 was designed to only amplify the predicted mutant transcript with
408 11bp insertion. Amplified PCR product were analysed using agarose gel electrophoresis and each
409 band was purified and sequenced.

410 Primer set 1: Forward: ATGCAGAGTCGGTACAAGGC; Reverse: CCGTTCGAGCTGACCTCATT

411 Primer set 2: Forward: CCTGGGGAACAAGTTTCTTT; Reverse: GTGCAAGGGGCTGTATCCTA

412

413 SDS-PAGE, Coomassie staining and Western blot

414 RBC ghosts were prepared by lysing mouse RBCs with ice-cold 5mM phosphate buffer (ph7.4) and
415 centrifuged at 20,000g for 20 minutes followed by removal of the supernatant. The pellet was
416 further washed with the 5mM phosphate buffer until the supernatant became clear. The RBC ghosts
417 or whole blood lysates were denatured in SDS-PAGE loading buffer (0.0625M Tris pH 6.8, 2% SDS, 10%
418 glycerol, 0.1M DTT, 0.01% bromophenol blue) at 95°C for 5 minutes before loading onto a Mini-
419 PROTEAN® TGX™ Precast Gels (Bio-Rad, Hercules, CA). The gels were then either stained with
420 Coomassie blue solution (45% v/v methanol, 7% v/v acetic acid, 0.25% w/v Brilliant Blue G) overnight
421 or transferred to a nitrocellulose membrane. The western blot was carried out using these primary
422 antibodies: anti-alpha 1 spectrin (clone 17C7), anti-beta 1 spectrin (clone 4C3) (Abcam, Cambridge,
423 UK), anti-GAPDH (clone 6C5) (Merck Millipore, Darmstadt, Germany), anti-N-terminal *Ank-1* "p89",
424 anti-Band 3 and anti-protein 4.2 (kind gifts from Connie Birkenmeier, Jackson Laboratory, US).

425

426 Malaria infection

427 250µl of thawed *P. chabaudi adami* infected blood was injected into the intraperitoneal cavity of a
428 C57BL/6 donor mouse. When the donor mouse reached 1-10% parasite load (parasitemia), blood
429 was collected through cardiac puncture. The parasitized blood was diluted with Krebs' buffered
430 saline with 0.2% glucose as described previously [50]. Each experimental mouse was infected with
431 $1x10^4$ parasites intraperitoneally. The parasitemia of these mice were monitored either using light
432 microscopy or flow cytometry.

433

434 Terminal deoxynucleotidyl transferase dUTP nick end labelling (TUNEL) staining

435 3µl of infected blood containing 1-10% parasitemia were collected during trophozoite stage and
436 fixed in 1 in 4 diluted BD Cytofix™ Fixation Buffer (BD Biosciences, Franklin Lakes, NJ) for at least day
437 until they were needed. Each sample was then washed twice with MT-PBS, and adhered to a glass
438 slide pre-coated with 0.1% polyethylenimine (PEI) for 10 minutes at room temperature. The excess
439 cells were washed off with the wash solution from APO-BrdU TUNEL assay kit (Thermo Scientific,
440 Waltham, MA) and incubated overnight at room temperature with TUNEL labelling solution (1mM
441 Cobalt Chloride, 25mM Tris-HCl pH 6.6, 200mM sodium cacodylate, 0.25mg/ml BSA, 60uM BrdUTP,
442 15U Terminal transferase). The slides were washed three times with rinse buffer from APO-BrdU
443 TUNEL assay kit, followed by staining with 50µg/ml of anti-BrdU-Biotin antibody (Novus Biologicals,
444 Littleton, CO) in MT-PBT (MT-PBS, 0.5% BSA, 0.05% Triton X-100) for 1 hour. The slides were then
445 washed three times with MT-PBT, followed by probing with 2µg/ml Alexa Fluor® 594 conjugated
446 streptavidin (Thermo Scientific, Waltham, MA). Next, they were washed three times with MT-PBS
447 and mounted with SlowFade® Gold antifade reagent with DAPI (Thermo Scientific, Waltham, MA)
448 and sealed. When the slides were dried, they were examined using Axioplan 2 fluorescence light
449 microscope (Carl Zeiss, Oberkochen, Germany) between 600x to 1000x magnification. At least 100

450 DAPI-positive cells were counted, and each was graded as either positive or negative for TUNEL
451 staining, as an indication of DNA fragmentation.

452

453 *In vivo* erythrocyte tracking (IVET) assays

454 The IVET assay was carried out as previously described by Lelliott, et al. [51,52]. Briefly, 1.5ml to 2ml of
455 whole blood was collected from wild-type and *Ank-1*$^{(MRI61689/+)}$ mice via cardiac puncture. Both wild-
456 type and *Ank-1*$^{(MRI61689/+)}$ blood were either stained with 10µg/ml of Atto 633 or 125µg/ml of EZ-
457 Link™ Sulfo-NHS-LC-Biotin (Biotin) (Thermo Scientific, Waltham, MA) for 45 minutes at room
458 temperature, followed by washing three times with MT-PBS. The *Ank-1*$^{(MRI61689/+)}$ blood was mixed
459 with wild-type blood in two different dye combinations to correct for any dye effects. $1x10^9$
460 erythrocytes were injected intravenously into infected wild-type mice at 1-5% parasitemia during
461 schizogony stage, usually 8-10 days post-infection with $1x10^4$ parasites. Blood samples were
462 collected at 30 minutes, 3hours, 12 hours, 20 hours and 36 hours after injection. The ratio of
463 infected *Ank-1*$^{(MRI61689/+)}$ to wild-type erythrocytes was determined on flow cytometry, as an
464 indication of the relative susceptibility to malaria infections between wild-type and *Ank-1*$^{(MRI61689/+)}$
465 mice. The proportion of labelled blood populations were also tracked over time to determine the
466 clearance of these RBCs from the circulation.

467

468 Flow cytometry analysis of blood samples

469 For both malaria infections and IVET assay, 2µl of whole blood samples were stained with 2µg/ml
470 streptavidin-PE-Cy7 (only for experiments with biotinylated erythrocytes), 1µg/ml anti-CD45–
471 allophycocyanin (APC)–eFluor 780 (clone 30-F11), 1µg/ml anti-CD71 (TFR1)–PerCP–eFluor 710 (clone
472 R17217) (eBioscience, San Diego, CA), 4µM Hoechst 33342 (Sigma-Aldrich, St Louis, MO) and 12µM
473 JC-1 (Thermo Scientific, Waltham, MA) in MTRC. All samples analysed through flow cytometry were

474 performed on BD LSRFortessa (BD Biosciences, Franklin Lakes, NJ), where 100,000 to 2,000,000
475 events were collected and visualized on FACSDiva™ and FlowJo software. The RBCs and leukocytes
476 were first selected on forward scatter and side scatter channels (FSC/SSC) signals, followed by gating
477 of single cells based on FS area to height ratio. RBCs were further isolated by gating on CD71
478 negative and CD45 negative population, followed by gating on Atto-labelled and Biotin-labelled
479 erythrocytes on appropriate channels (APC for Atto-633, PE for Atto-565 and PE-Cy7 for Biotin). The
480 parasitemia of each labelled erythrocyte population was determined by gating on Hoechst 33342
481 positive and JC-1 positive population.

482

483 Statistical analysis

484 The LOD score method coupled with Bonferroni correction was used to determine the causative
485 mutation for MRI61689. The statistical significance of the malaria survival was tested using the Log-
486 Rank test. The statistical significance of parasite infection was determined via the statmod software
487 package for R (http://bioinf.wehi.edu.au/software/compareCurves) using the
488 'compareGrowthCurves' function with 10,000 permutation, followed by adjustments for multiple
489 testing. The statistical significance for the ratios of IVET assays was determined using the one sample
490 t-test with hypothetical mean of 1. For the rest of the results, statistical significance was determined
491 using two-tailed Students t-tests.

492

493 **References**

494 1 W.H.O. *World Malaria Report 2015*. (World Health Organisation (WHO), 2015).
495 2 Kwiatkowski, D. P. How malaria has affected the human genome and what human genetics
496 can teach us about malaria. *Am J Hum Genet* **77**, 171-192 (2005).
497 3 Piel, F. B. *et al.* Global distribution of the sickle cell gene and geographical confirmation of
498 the malaria hypothesis. *Nature communications* **1**, 104, doi:10.1038/ncomms1104 (2010).
499 4 Carter, R. & Mendis, K. N. Evolutionary and historical aspects of the burden of malaria. *Clin*
500 *Microbiol Rev* **15**, 564-594 (2002).

501 5 Zimmerman, P. A. *et al.* Emergence of FY*A(null) in a Plasmodium vivax-endemic region of
502 Papua New Guinea. *Proc Natl Acad Sci U S A* **96**, 13973-13977 (1999).
503 6 Miller , L. H., Mason , S. J., Clyde , D. F. & McGinniss , M. H. The Resistance Factor to
504 Plasmodium vivax in Blacks. *New England Journal of Medicine* **295**, 302-304,
505 doi:doi:10.1056/NEJM197608052950602 (1976).
506 7 Cyrklaff, M. *et al.* Hemoglobins S and C interfere with actin remodeling in Plasmodium
507 falciparum-infected erythrocytes. *Science* **334**, 1283-1286, doi:10.1126/science.1213775
508 (2011).
509 8 Allen, S. J. *et al.* Prevention of cerebral malaria in children in Papua New Guinea by
510 southeast Asian ovalocytosis band 3. *Am J Trop Med Hyg* **60**, 1056-1060 (1999).
511 9 Jarolim, P. *et al.* Deletion in erythrocyte band 3 gene in malaria-resistant Southeast Asian
512 ovalocytosis. *Proceedings of the National Academy of Sciences of the United States of*
513 *America* **88**, 11022-11026 (1991).
514 10 Mgone, C. S. *et al.* Occurrence of the erythrocyte band 3 (AE1) gene deletion in relation to
515 malaria endemicity in Papua New Guinea. *Trans R Soc Trop Med Hyg* **90**, 228-231 (1996).
516 11 Genton, B. *et al.* Ovalocytosis and cerebral malaria. *Nature* **378**, 564-565,
517 doi:10.1038/378564a0 [doi] (1995).
518 12 Lecomte, M. C. *et al.* [Hereditary elliptocytosis in West Africa: frequency and repartition of
519 spectrin variants]. *C R Acad Sci III* **306**, 43-46 (1988).
520 13 Facer, C. A. Erythrocytes carrying mutations in spectrin and protein 4.1 show differing
521 sensitivities to invasion by Plasmodium falciparum. *Parasitol Res* **81**, 52-57 (1995).
522 14 Kidson, C., Lamont, G., Saul, A. & Nurse, G. T. Ovalocytic erythrocytes from Melanesians are
523 resistant to invasion by malaria parasites in culture. *Proceedings of the National Academy of*
524 *Sciences of the United States of America* **78**, 5829-5832 (1981).
525 15 Hadley, T. *et al.* Resistance of Melanesian elliptocytes (ovalocytes) to invasion by
526 Plasmodium knowlesi and Plasmodium falciparum malaria parasites in vitro. *J Clin Invest* **71**,
527 780-782 (1983).
528 16 Schulman, S. *et al.* Growth of Plasmodium falciparum in human erythrocytes containing
529 abnormal membrane proteins. *Proc Natl Acad Sci U S A* **87**, 7339-7343 (1990).
530 17 Chishti, A. H., Palek, J., Fisher, D., Maalouf, G. J. & Liu, S. C. Reduced invasion and growth of
531 Plasmodium falciparum into elliptocytic red blood cells with a combined deficiency of
532 protein 4.1, glycophorin C, and p55. *Blood* **87**, 3462-3469 (1996).
533 18 Cortes, A., Benet, A., Cooke, B. M., Barnwell, J. W. & Reeder, J. C. Ability of Plasmodium
534 falciparum to invade Southeast Asian ovalocytes varies between parasite lines. *Blood* **104**,
535 2961-2966, doi:10.1182/blood-2004-06-2136 2004-06-2136 [pii] (2004).
536 19 Dua, M., Raphael, P., Sijwali, P. S., Rosenthal, P. J. & Hanspal, M. Recombinant falcipain-2
537 cleaves erythrocyte membrane ankyrin and protein 4.1. *Mol Biochem Parasitol* **116**, 95-99
538 (2001).
539 20 Nicolas, V. *et al.* Rh-RhAG/Ankyrin-R, a New Interaction Site between the Membrane Bilayer
540 and the Red Cell Skeleton, Is Impaired by Rhnull-associated Mutation. *Journal of Biological*
541 *Chemistry* **278**, 25526-25533, doi:10.1074/jbc.M302816200 (2003).
542 21 Grey, J. L., Kodippili, G. C., Simon, K. & Low, P. S. Identification of contact sites between
543 ankyrin and band 3 in the human erythrocyte membrane. *Biochemistry* **51**, 6838-6846,
544 doi:10.1021/bi300693k (2012).
545 22 Su, Y. *et al.* Associations of protein 4.2 with band 3 and ankyrin. *Molecular and cellular*
546 *biochemistry* **289**, 159-166, doi:10.1007/s11010-006-9159-x (2006).
547 23 Eber, S. W. *et al.* Ankyrin-1 mutations are a major cause of dominant and recessive
548 hereditary spherocytosis. *Nat Genet* **13**, 214-218, doi:10.1038/ng0696-214 (1996).
549 24 Casale, M. & Perrotta, S. Splenectomy for hereditary spherocytosis: complete, partial or not
550 at all? *Expert review of hematology* **4**, 627-635, doi:10.1586/ehm.11.51 (2011).

551 25 Godal, H. C. & Heisto, H. High prevalence of increased osmotic fragility of red blood cells
552 among Norwegian blood donors. *Scandinavian journal of haematology* **27**, 30-34 (1981).
553 26 Eber, S. W., Pekrun, A., Neufeldt, A. & Schroter, W. Prevalence of increased osmotic fragility
554 of erythrocytes in German blood donors: screening using a modified glycerol lysis test.
555 *Annals of hematology* **64**, 88-92 (1992).
556 27 Jensson, O., Jonasson, J. L. & Magnusson, S. Studies on herediatary spherocytosis in Iceland.
557 *Acta medica Scandinavica* **201**, 187-195 (1977).
558 28 Yawata, Y. *et al.* Characteristic features of the genotype and phenotype of hereditary
559 spherocytosis in the Japanese population. *Int J Hematol* **71**, 118-135 (2000).
560 29 Glele-Kakai, C. *et al.* Epidemiological studies of spectrin mutations related to hereditary
561 elliptocytosis and spectrin polymorphisms in Benin. *Br J Haematol* **95**, 57-66 (1996).
562 30 Shear, H. L., Roth, E. F., Jr., Ng, C. & Nagel, R. L. Resistance to malaria in ankyrin and spectrin
563 deficient mice. *Br J Haematol* **78**, 555-560 (1991).
564 31 Greth, A. *et al.* A novel ENU-mutation in ankyrin-1 disrupts malaria parasite maturation in
565 red blood cells of mice. *PLoS One* **7**, e38999, doi:10.1371/journal.pone.0038999 (2012).
566 32 Rank, G. *et al.* Novel roles for erythroid Ankyrin-1 revealed through an ENU-induced null
567 mouse mutant. *Blood* **113**, 3352-3362, doi:blood-2008-08-172841 [pii] 10.1182/blood-2008-
568 08-172841 (2009).
569 33 Stephens, R., Culleton, R. L. & Lamb, T. J. The contribution of *Plasmodium chabaudi* to our
570 understanding of malaria. *Trends in Parasitology* **28**, 73-82, doi:10.1016/j.pt.2011.10.006
571 (2012).
572 34 Ayi, K., Turrini, F., Piga, A. & Arese, P. Enhanced phagocytosis of ring-parasitized mutant
573 erythrocytes: a common mechanism that may explain protection against falciparum malaria
574 in sickle trait and beta-thalassemia trait. *Blood* **104**, 3364-3371, doi:10.1182/blood-2003-11-
575 3820 (2004).
576 35 McMorran, B. J. *et al.* Platelets Kill Intraerythrocytic Malarial Parasites and Mediate Survival
577 to Infection. *Science* **323**, 797-800, doi:10.1126/science.1166296 (2009).
578 36 Gallagher, P. G. Hematologically important mutations: ankyrin variants in hereditary
579 spherocytosis. *Blood Cells Mol Dis* **35**, 345-347, doi:10.1016/j.bcmd.2005.08.008 (2005).
580 37 Nakanishi, H., Kanzaki, A., Yawata, A., Yamada, O. & Yawata, Y. Ankyrin gene mutations in
581 japanese patients with hereditary spherocytosis. *Int J Hematol* **73**, 54-63 (2001).
582 38 Edelman, E. J., Maksimova, Y., Duru, F., Altay, C. & Gallagher, P. G. A complex splicing defect
583 associated with homozygous ankyrin-deficient hereditary spherocytosis. *Blood* **109**, 5491-
584 5493, doi:10.1182/blood-2006-09-046573 (2007).
585 39 Kyrylkova, K., Kyryachenko, S., Leid, M. & Kioussi, C. Detection of apoptosis by TUNEL assay.
586 *Methods Mol Biol* **887**, 41-47, doi:10.1007/978-1-61779-860-3_5 (2012).
587 40 Straat, M., van Bruggen, R., de Korte, D. & Juffermans, N. P. Red blood cell clearance in
588 inflammation. *Transfusion medicine and hemotherapy : offizielles Organ der Deutschen*
589 *Gesellschaft fur Transfusionsmedizin und Immunhamatologie* **39**, 353-361,
590 doi:10.1159/000342229 (2012).
591 41 Jakeman, G., Saul, A., Hogarth, W. & Collins, W. Anaemia of acute malaria infections in non-
592 immune patients primarily results from destruction of uninfected erythrocytes. *Parasitology*
593 **119**, 127-133 (1999).
594 42 Lamikanra, A. A. *et al.* Malarial anemia: of mice and men. *Blood* **110**, 18-28 (2007).
595 43 Dondorp, A. M. *et al.* Prognostic significance of reduced red blood cell deformability in
596 severe falciparum malaria. *Am J Trop Med Hyg* **57**, 507-511 (1997).
597 44 Dondorp, A. *et al.* The role of reduced red cell deformability in the pathogenesis of severe
598 falciparum malaria and its restoration by blood transfusion. *Transactions of the Royal Society*
599 *of Tropical Medicine and Hygiene* **96**, 282-286 (2002).
600 45 Deplaine, G. *et al.* The sensing of poorly deformable red blood cells by the human spleen can
601 be mimicked in vitro. *Blood* **117**, e88-95, doi:10.1182/blood-2010-10-312801 (2011).

602 46 Hortle, E. *et al.* Adenosine monophosphate deaminase 3 activation shortens erythrocyte
603 half-life and provides malaria resistance in mice. *Blood*, doi:10.1182/blood-2015-09-666834
604 (2016).
605 47 Bauer, D. C., McMorran, B. J., Foote, S. J. & Burgio, G. Genome-wide analysis of chemically
606 induced mutations in mouse in phenotype-driven screens. *BMC Genomics* **16**, 1-8,
607 doi:10.1186/s12864-015-2073-4 (2015).
608 48 Wang, K., Li, M. & Hakonarson, H. ANNOVAR: functional annotation of genetic variants from
609 high-throughput sequencing data. *Nucleic Acids Research* **38**, e164-e164,
610 doi:10.1093/nar/gkq603 (2010).
611 49 Livak, K. J. & Schmittgen, T. D. Analysis of relative gene expression data using real-time
612 quantitative PCR and the 2− ΔΔCT method. *methods* **25**, 402-408 (2001).
613 50 Jarra, W. & Brown, K. Protective immunity to malaria: studies with cloned lines of
614 Plasmodium chabaudi and P. berghei in CBA/Ca mice. I. The effectiveness and inter‐and
615 intra‐species specificity of immunity induced by infection. *Parasite immunology* **7**, 595-606
616 (1985).
617 51 Lelliott, P. M., Lampkin, S., McMorran, B. J., Foote, S. J. & Burgio, G. A flow cytometric assay
618 to quantify invasion of red blood cells by rodent Plasmodium parasites in vivo. *Malar J* **13**,
619 100, doi:10.1186/1475-2875-13-100 (2014).
620 52 Lelliott, P. M., McMorran, B. J., Foote, S. J. & Burgio, G. In vivo assessment of rodent
621 Plasmodium parasitemia and merozoite invasion by flow cytometry. *JoVE (Journal of*
622 *Visualized Experiments)*, e52736-e52736 (2015).

623

624 **Acknowledgement**

625 We would like to acknowledge Shelley Lampkin and Australian Phenomics Facility (APF) for the
626 maintenance of the mouse colonies. This study was funded by the National Health and Medical
627 Research Council of Australia (Program Grant 490037, and Project Grants 605524 and APP1047090),
628 Australian Society of Parasitology (ASP), OzEMalaR, National Collaborative Research Infrastructure
629 Strategy (NCRIS), the Education Investment Fund from the Department of Education and Training,
630 the Australian Phenomics Network, Howard Hughes Medical Institute and the Bill and Melinda Gates
631 Foundation. We would finally like to thanks two anonymous reviewers for their insightful comments
632 on this manuscript.

633

634

635

636 **Figure Legends**

637 **Figure 1**. **The phenotypic characterisation of *Ank-1*$^{(MRI61689/+)}$ mice.** The morphology of *Ank-1*$^{(MRI61689/+)}$
638 and *Ank-1*$^{(MRI61689/MRI61689)}$ erythrocytes under light microscopy with Giemsa stain (a) and scanning
639 electron microscopy (b). The osmotic fragility curve of wild-type and *Ank-1*$^{(MRI61689/+)}$ erythrocytes
640 when subjected to osmotic stress (c) (n=5-7 per group). The *in-vitro* spleen retention rate of wild-
641 type and *Ank-1*$^{(MRI61689/+)}$ erythrocytes when passing through filter beds (d) (n=3 per group). **
642 indicates P<0.01, *** indicates P<0.001, and all error bars are standard error of mean (SEM).

643

644 **Figure 2**. **The identification of *Ank-1*$^{(MRI61689)}$ mutation and its effects on transcription.** The
645 sequencing of *Ank-1*$^{(MRI61689)}$ mutation, showing a T to A transversion (a). Gel electrophoresis of
646 amplified cDNA product from wild-type, *Ank-1*$^{(MRI61689/+)}$ and *Ank-1*$^{(MRI61689/MRI61689)}$ embryonic livers
647 with primers that spanned the exon 17 to 21 of ankyrin-1 cDNA (primer set 1) (b). The sequencing
648 results of both bands, showing exon skipping in the abnormal transcript of *Ank-1*$^{(MRI61689/MRI61689)}$
649 embryonic liver (c). Gel electrophoresis of amplified cDNA product from wild-type, *Ank-1*$^{(MRI61689/+)}$
650 and *Ank-1*$^{(MRI61689/MRI61689)}$ embryonic livers with primers that contained the predicted 11bp insertion
651 (primer set 2) (d). Sequencing result showing an 11bp insertion between exon 17 and 18 cDNA of the
652 *Ank-1*$^{(MRI61689)}$ transcript (e). The predicted effect of the insertion on the translation of ankyrin-1,
653 showing a frameshift and a premature chain termination (f).

654

655 **Figure 3**. **The effect of *Ank-1*$^{(MRI61689)}$ mutation on the *Ank-1* expression.** Quantitative PCR showing
656 the ankyrin-1 mRNA levels in both *Ank-1*$^{(MRI61689/+)}$ and *Ank-1*$^{(MRI61689/MRI61689)}$ embryonic liver (a). The
657 protein levels of various cytoskeletal proteins examined with both Coomassie (b) and Western blot
658 (c). The relative protein levels of ankyrin-1 calculated from the western blot (d) (n=3 per group).
659 Error bars indicate SEM.

660

661 **Figure 4**. **The response of *Ank-1*$^{(MRI61689/+)}$ mice to malaria infection.** The parasite load of wild-type
662 and *Ank-1*$^{(MRI61689/+)}$ mice when infected with 1x10^{4} *P. chabaudi* (a) and the associated survival curve
663 (b). To determine the mechanisms of resistance, parasite intra-erythrocytic growth was assessed
664 through TUNEL assay at 1-10% parasitemia during late trophozoite stage, as visualised from
665 immunofluorescent images showing presence of parasites and TUNEL-positive parasites (c). The
666 number of TUNEL-positive parasites in both wild-type and *Ank-1*$^{(MRI61689/+)}$ mice were counted and
667 expressed as a percentage (d) (n=3). For parasite invasion and RBC clearance, The IVET assay was
668 done showing the ratio of infected *Ank-1*$^{(MRI61689/+)}$ to wild-type erythrocytes over 36 hours (e) and
669 the relative number *Ank-1*$^{(MRI61689/+)}$ and wild-type erythrocyte in both infected and uninfected mice
670 (f) during *P. chabaudi* infection (n=7). ** indicates P<0.01, *** indicates P<0.001, ## and ###
671 indicates P<0.01 and P<0.001 respectively when compared to wild-type RBC number in infected mice,
672 whereas ^^ indicates P<0.01 when compared to *Ank-1*$^{(MRI61689/+)}$ RBC number in uninfected mice.
673 Error bars indicate SEM.

674

675 **Tables**

	WBC ($x10^6$ /ml)	RBC ($x10^9$ /ml)	HGB (g/L)	MCV (fL)	MCH (pg)	MCHC (g/L)	PLT ($x10^6$ /ml)	%Retics
Wild type	8.7±0.5	10.5±0.1	153.2±2.2	51.4±0.4	14.6±0.1	283.6±2.8	1151±57	2.69±0.26
Ank-1$^{(MRI61689/+)}$	11.9±4.5	11.1±0.1	151.2±1.4	46.1±0.2	13.5±0.1	281.4±9.3	1151±61	2.24±0.21
p-values	NS	P<0.01	NS	P<0.001	P<0.001	NS	NS	NS

676

677 **Table 1**. **The complete blood count of *Ank-1*$^{(MRI61689/+)}$ mice.** The haematological parameters of *Ank-*
678 *1*$^{(MRI61689/+)}$ compared to wild-type mice (n=19-25). WBC = white blood cell count; RBC = red blood cell
679 count; HGB = haemoglobin; MCV = mean corpuscular volume; MCH = mean corpuscular
680 haemoglobin; MCHC = mean corpuscular haemoglobin concentration; PLT = platelet
681 concentration; %Retics = percentage of reticulocytes.

682

Chromosome	Gene name	Location	Reference base	Variant base	Number of mutant mice with mutation	LOD score (Threshold: 2.08)
9	Acp5	22129643	C	A	(3/8)	-0.32
8	Kcnk1	126025024	C	T	(4/8)	0
17	Epas1	86825679	A	T	(0/8)	-2.33
7	Picalm	90165538	G	T	(0/8)	-2.33
18	Socs6	88869240	A	G	(5/8)	0.32
8	Ank1	23106019	T	A	(8/8)	2.33

683

684 **Table 2: The identification of MRI61689 mutation.** Six variants were selected from the exome
685 sequencing, each mutation was sequenced in *Ank-1*$^{(MRI61689/+)}$ mice and the number of mutant mice
686 carrying each mutation was determined and LOD score was calculated, with LOD threshold being
687 2.08 (n=8).

688

689

Figure 1

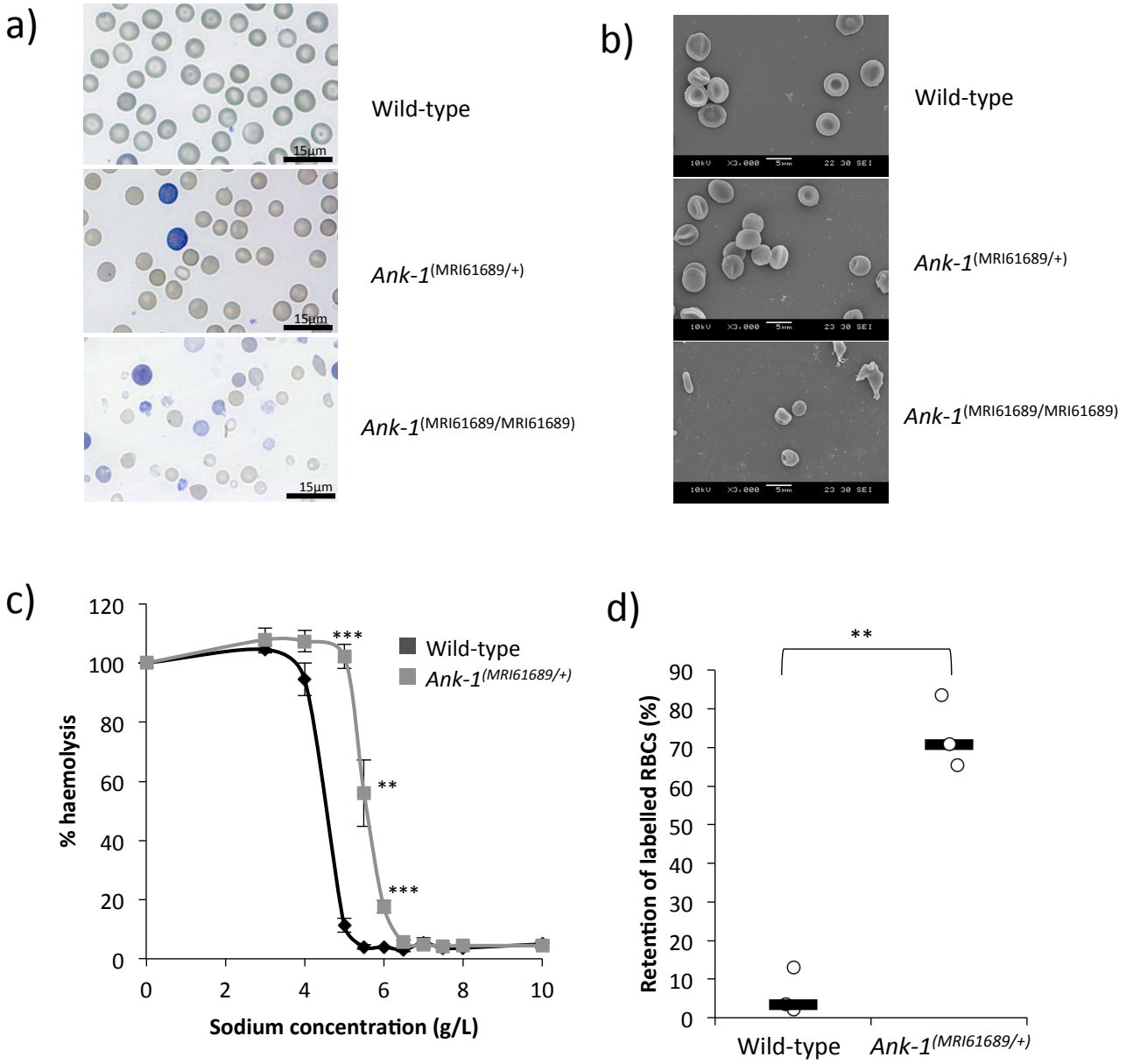
a)
15µm
Wild-type
Ank-1(MRI61689/+)
Ank-1(MRI61689/MRI61689)
b)
Wild-type
Ank-1(MRI61689/+)
Ank-1(MRI61689/MRI61689)
c)
% haemolysis
Sodium concentration (g/L)
Wild-type
Ank-1(MRI61689/+)
***
**
d)
Retention of labelled RBCs (%)
Wild-type
Ank-1(MRI61689/+)
**

Figure 2

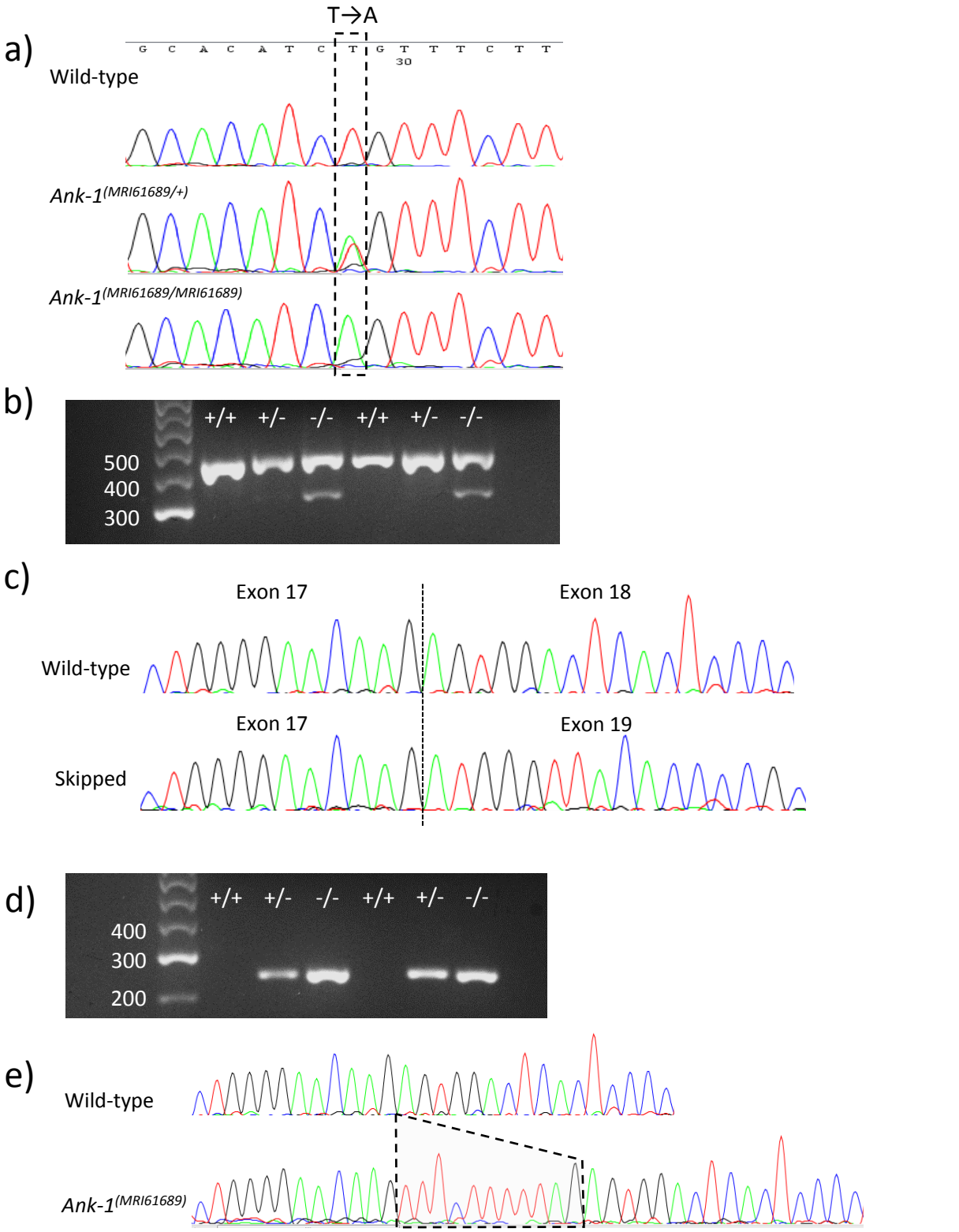

f)

Wild-type gca cat ctg ttt ctt ttt ag AGT GGA CTC ACT CCC
---------- Ser Gly Leu Thr Pro

Ank-1(MRI61689) gca cat cag TTT CTT TTT AGA GTG GAC TCA CTC CC……TGA
---------- Phe Leu Phe Arg Val Asp Ser Leu……STOP

Figure 3

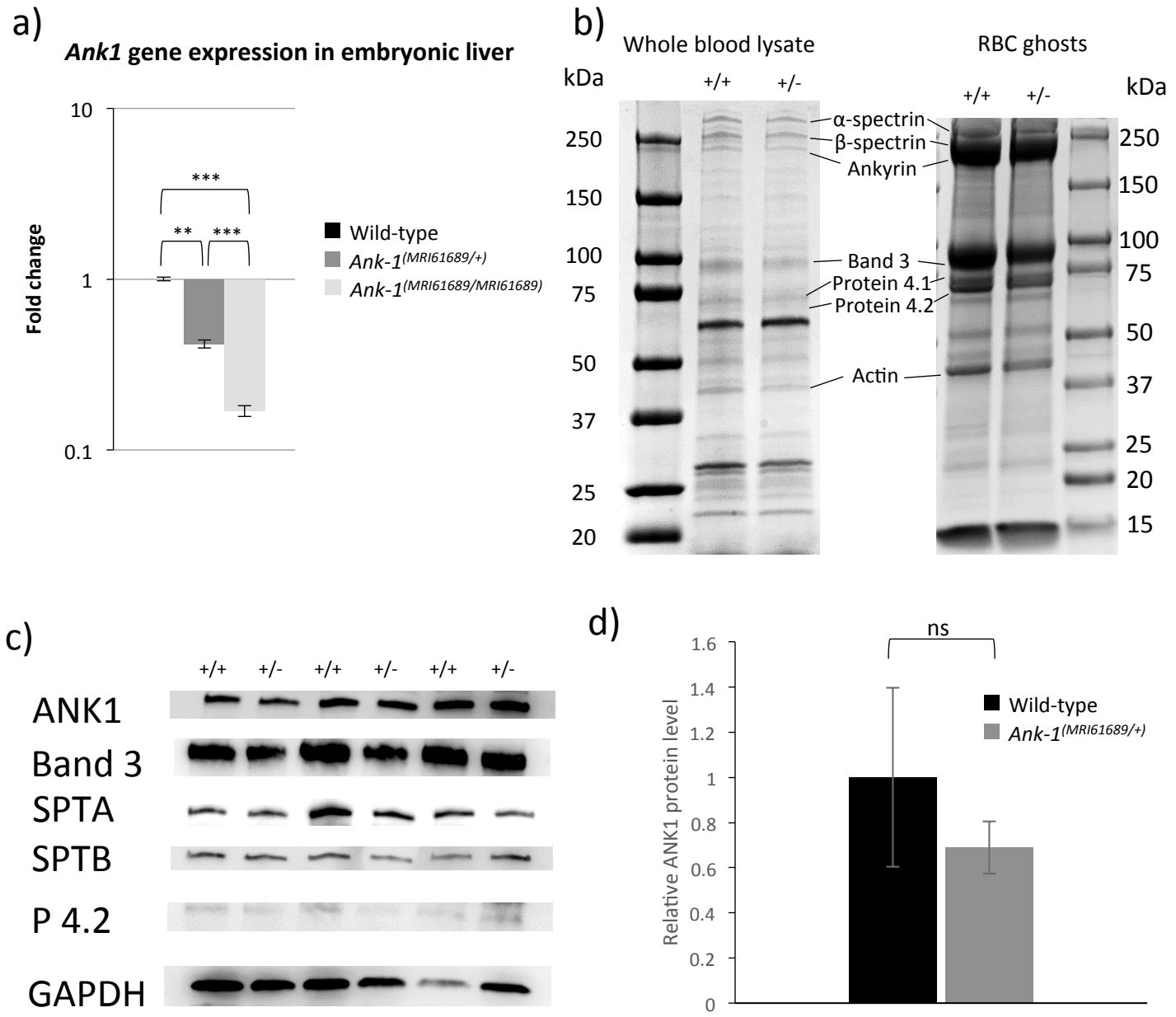
a)
Ank1 gene expression in embryonic liver
Fold change
10
1
0.1
***
**
***
Wild-type
Ank-1(MRI61689/+)
Ank-1(MRI61689/MRI61689)
b)
Whole blood lysate
RBC ghosts
kDa
+/+
+/-
250
150
100
75
50
37
25
20
α-spectrin
β-spectrin
Ankyrin
Band 3
Protein 4.1
Protein 4.2
Actin
15
c)
ANK1
Band 3
SPTA
SPTB
P 4.2
GAPDH
d)
ns
Relative ANK1 protein level
1.6
1.4
1.2
1
0.8
0.6
0.4
0.2
0
Wild-type
Ank-1(MRI61689/+)

Figure 4

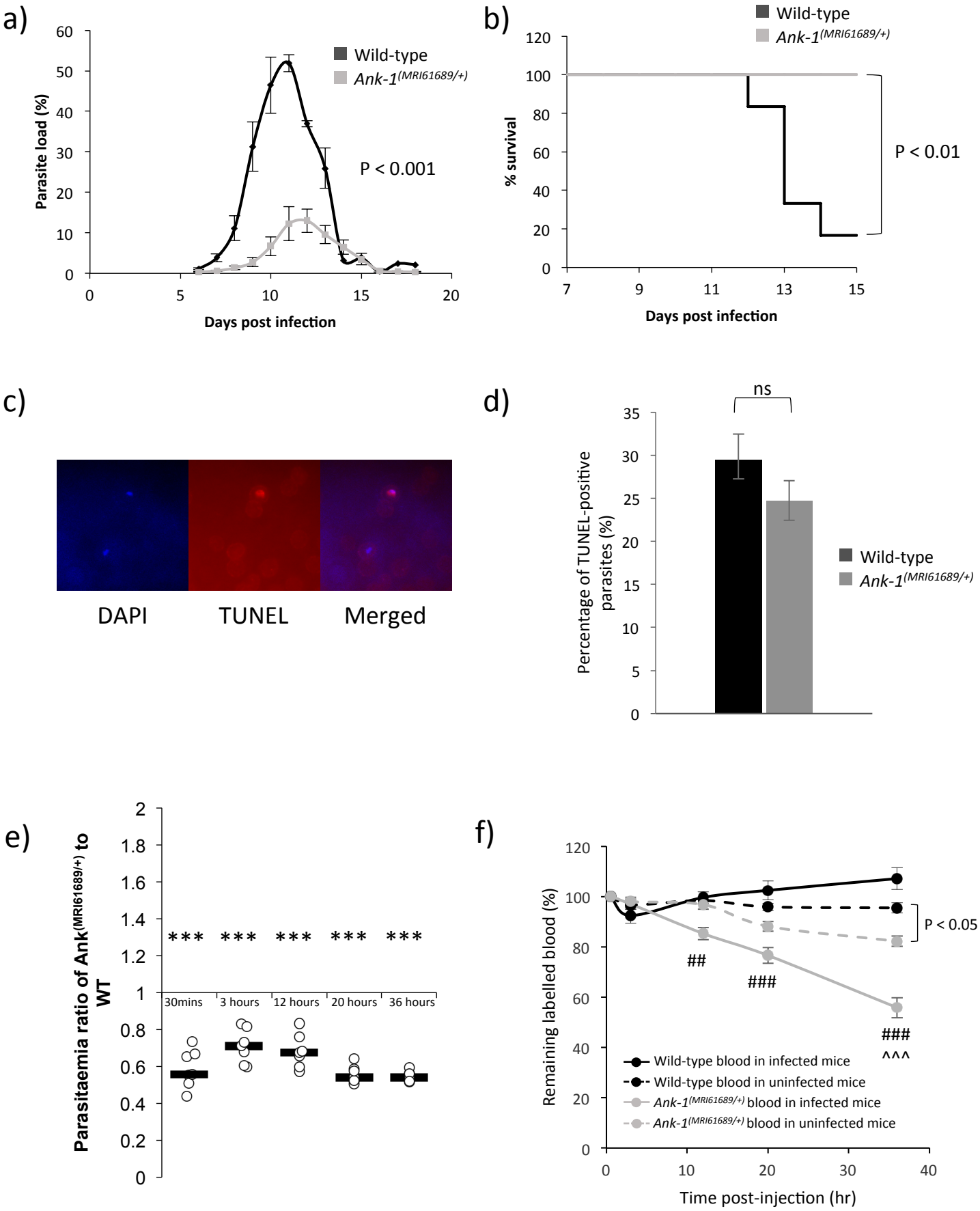
a)
Parasite load (%)
Days post infection
Wild-type
Ank-1(MRI61689/+)
P < 0.001
b)
% survival
Days post infection
Wild-type
Ank-1(MRI61689/+)
P < 0.01
c)
DAPI
TUNEL
Merged
d)
Percentage of TUNEL-positive parasites (%)
ns
Wild-type
Ank-1(MRI61689/+)
e)
Parasitaemia ratio of Ank(MRI61689/+) to WT
30mins
3 hours
12 hours
20 hours
36 hours
***
f)
Remaining labelled blood (%)
Time post-injection (hr)
P < 0.05
##
###
^^^
Wild-type blood in infected mice
Wild-type blood in uninfected mice
Ank-1(MRI61689/+) blood in infected mice
Ank-1(MRI61689/+) blood in uninfected mice

Supplementary figure 1

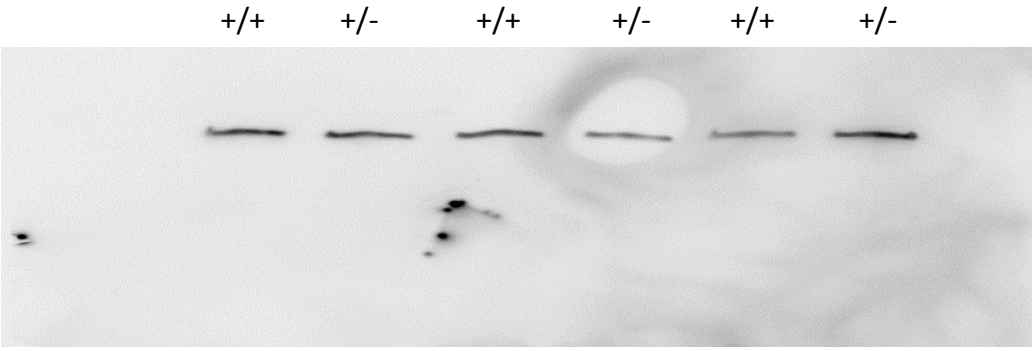

Supplementary figure 1. **The full western blot membrane when probed with anti-beta-spectrin antibody.** The disparity of band intensity as shown in Figure 3c is due to uneven surface of the membrane rather than post-processing issue.

Supplementary figure 2

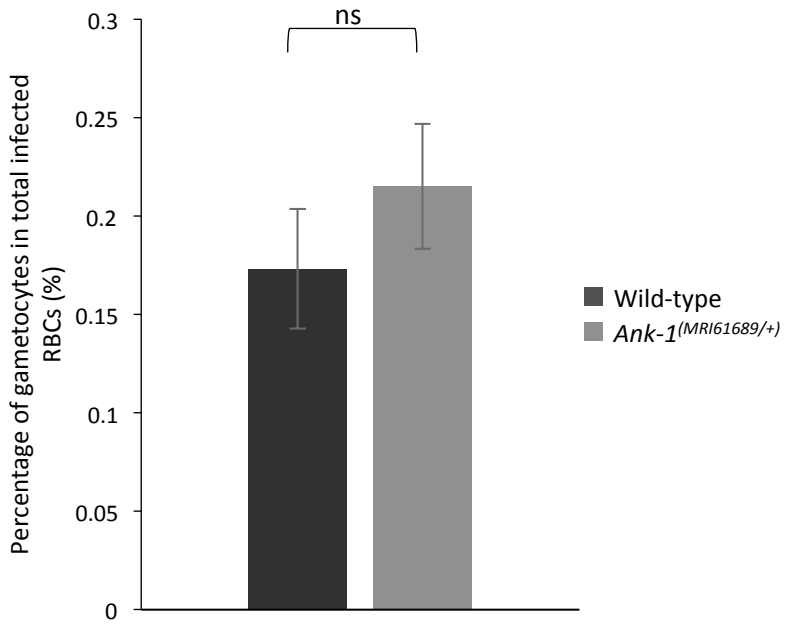

Supplementary figure 2. **The percentage of gametocytes of wild-type and of *Ank-1*$^{(MRI61689/+)}$ mice during malaria infection.** Parasite gametocyte numbers were counted under light microscopy at 15-30% parasitaemia, and the proportion of gametocytes to total infected RBCs were calculated (n=6). Error bars indicate SEM.

Supplementary figure 3

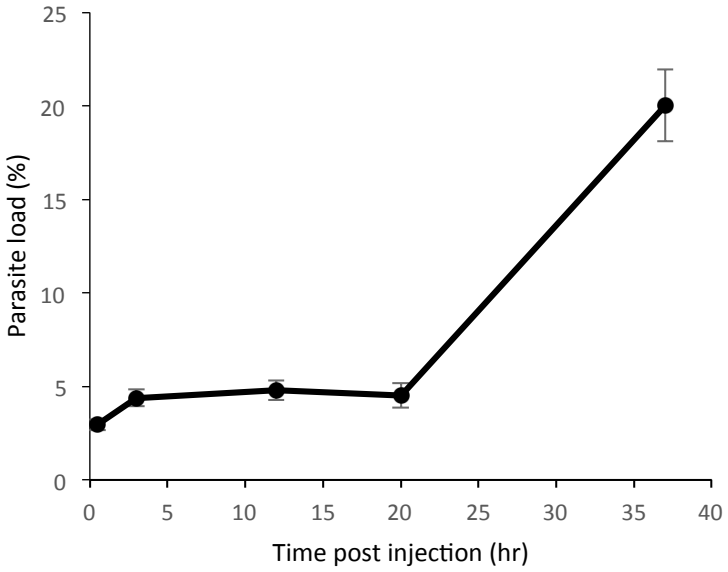

Supplementary figure 3. **The parasite load of the mice during IVET assays.** The parasite load of the host mice during IVET assay (n=7). Error bars indicate SEM.